Local flow structure of turbulence in three, four, and five dimensions

T. Yamamoto, H. Shimizu, T. Inoshita, and T. Nakano
Department of Physics, Chuo University, 1-13-27 Kasuga, Bunkyo-ku, Tokyo 113-8851, Japan

T. Gotoh*
Department of Scientific and Engineering Simulation, Graduate School of Engineering, Nagoya Institute of Technology, Gokiso, Showa-ku, Nagoya 466-8555, Japan

(Received 24 March 2012; revised manuscript received 4 October 2012; published 22 October 2012)

Probability density functions (PDF's) of the eigenvalues of the strain tensor of an incompressible isotropic turbulence in 3, 4, and 5 dimensions are computed by direct numerical simulation of Navier-Stokes equations. The PDF's of the smallest (negative) eigenvalue are found to be wider than those of the other ones in all dimensions and to be very insensitive to the dimension. In any dimension, the eigenvalues other than the lowest one increase as the lowest one decreases, so that they tend to be positive for the large magnitude of the lowest eigenvalue. In such a situation the flow comes in along a single direction and comes out in the other directions, which is consistent with the dynamics of the Burgers turbulence in d dimensions. It is suggested that a driving motor of most intermittent turbulent structure is the compression along a single direction. For the velocity 2 form the conditional averages of the enstrophy and the total squared strain in three dimensions are computed as functions of the smallest eigenvalue and found to be monotonically increasing as the magnitude of the smallest eigenvalue increases. Also, it is found that PDF of the source term of the Poisson equation for the pressure is positively skewed but tends to be symmetric with increase of the spatial dimension. Dimension effects on the dynamics of the most compressible eigenvalue are argued.

DOI: 10.1103/PhysRevE.86.046320 PACS number(s): 47.27.Gs, 05.20.Jj, 47.27.ek

I. INTRODUCTION

In the study of turbulence there have been many efforts to search for something reasonable to approach from the well known and tractable state such as the multivariate Gaussian field by perturbative expansion or nonlinear mapping and so on, as inspired by the success in the statistical mechanics and quantum field theory. One way is to examine the dimension effects [1–7]. The effects of the spatial dimension on turbulence have been studied theoretically and numerically, and it was suggested that as the spatial dimension increases the incompressibility condition becomes less restrictive and larger (negative) longitudinal velocity gradient tends to be more probable than in three dimensions due to the local compressible strain, implying that the energy transfer toward high wavenumbers is enhanced and the local dynamics becomes closer to that of Burgers turbulence [1,8–11]. In the Burgers turbulence the shock structure is formed and the energy dissipation occurs in a thin layer of the shock so that the scaling exponent of the velocity structure function saturates at large order, the maximal intermittency.

This motivates us to examine the local flow structure in homogeneous isotropic turbulence in 3, 4, and 5 dimensions and to get insight into the role of spatial dimensions on the dynamics and statistical laws of turbulence, from which we may be able to find hints to develop a new theoretical approach to turbulence. In 3D turbulence, for instance, the ensemble of strong vortices is developed and a model of Burgers vortices [12] is proposed to embody such a turbulent flow that the fluid flows in radially and flows out along an axial direction of a strong vortex tube amplifying the vorticity. This model suggests that the straining motion plays a key fundamental role to transfer the energy to smaller scales of motion by squeezing a fluid blob or vortex. Such a structure can be analyzed in local coordinates in which the strain tensor is diagonal; one can easily imagine flow structure that a flow element is stretched along some axial directions, flowing in from the other directions even when the spatial dimensions are increased. In order to understand the role of spatial dimensions in the Navier-Stokes hydrodynamics, it is important and useful to examine in this frame how strong and frequent the squeezing and stretching action occur and how their relative ratios vary when the spatial dimension changes. To obtain a common picture as to the flow structure that holds in any dimension, we extend the dimension of turbulence to 3, 4, and 5, because the additional invariants other than the energy, which is conserved through the nonlinear term in the Navier-Stokes equations, are dependent on the parity of the dimension [8].

The NS equations of incompressible decaying turbulence are simulated for dimensions from three to five using the spectral method. Then we investigate the distributions of eigenvalues of the strain field from a point of view of comparing those among different dimensions. The fluid elements are locally compressed along directions of the negative eigenvalues and stretched along directions of the positive ones. Hence, the distribution of the eigenvalues can reveal the local flow structure. Such a study for various dimensions enables us to know the universal flow structure independent of dimension.

We obtained the following observations. The normalized probability density functions (PDF's) of the lowest (negative) eigenvalue are wider than those of the highest (positive) ones in all dimensions. The normalized PDF's of the lowest eigenvalue are independent of the dimension, so that the compression mechanism is universal irrespective of the dimension. In any dimension, the eigenvalues other than the lowest one increase

*gotoh.toshiyuki@nitech.ac.jp

as the latter decreases, so that they are positive for the large magnitude of the lowest eigenvalue. In such a situation, the flow comes in along a single direction and comes out in the other directions. A driving motor of turbulence is the compression along a single direction, which is the steepening mechanism in Burgers equation in one dimension.

The present paper is organized as follows. In Sec. II the basic equations for any dimension is presented. Section III is devoted to the analysis of the eigenvalues of the strain field. The lowest one is shown to play a crucial role of scaling other components. In Sec. IV the velocity 2 form, which is the antisymmetric tensor of the velocity derivative, is examined based on the lowest eigenvalue. Discussion and conclusion are given in Sec. V.

II. BASIC EQUATIONS

The Navier-Stokes equations of an incompressible fluid are given as

$$\frac{\partial u_i}{\partial t} + u_j \frac{\partial u_i}{\partial x_j} = -\frac{1}{\rho}\frac{\partial p}{\partial x_i} + \nu \Delta u_i, \tag{2.1}$$

$$\frac{\partial u_j}{\partial x_j} = 0, \tag{2.2}$$

where u_i is the velocity field, p the pressure, ρ the mass density, and ν the molecular viscosity, and the summation convention is assumed for the repeated indexes otherwise stated. The velocity derivative $\partial u_i/\partial x_j$ is conveniently decomposed into the symmetric and antisymmetric part as

$$\frac{\partial u_i}{\partial x_j} = s_{ij} + \frac{1}{2}\Omega_{ij}, \tag{2.3}$$

where

$$s_{ij} = \frac{1}{2}\left(\frac{\partial u_i}{\partial x_j} + \frac{\partial u_j}{\partial x_i}\right), \tag{2.4}$$

$$\Omega_{ij} = \frac{\partial u_i}{\partial x_j} - \frac{\partial u_j}{\partial x_i}. \tag{2.5}$$

Although Ω_{ij} is related to the vorticity field $\boldsymbol{\omega}$ in three dimensions as

$$\omega_i = -\tfrac{1}{2}\varepsilon_{ijk}\Omega_{jk}, \tag{2.6}$$

we use the antisymmetric form of Ω_{ij} in parallel to s_{ij} in an arbitrary dimension.

The equations for s_{ij} become

$$\frac{ds_{ij}}{dt} = \frac{1}{4}\Omega_{ik}\Omega_{jk} - s_{ik}s_{jk} - \frac{\partial^2 p}{\partial x_i \partial x_j} + \nu \Delta s_{ij}, \tag{2.7}$$

where

$$\frac{d}{dt} = \frac{\partial}{\partial t} + u_k \frac{\partial}{\partial x_k}$$

is the Lagrangian derivative in the moving frame. The equation for the pressure is obtained by setting j equal to i and taking the summation over i in Eq. (2.7);

$$\Delta p = \tfrac{1}{4}\Omega_{jk}^2 - s_{jk}^2 \equiv Q, \tag{2.8}$$

where the incompressible condition $s_{jj} = 0$ is used. Taking the spatial average of Eq. (2.8) leads to

$$\langle Q \rangle = 0 \tag{2.9}$$

by homogeneity.

On the other hand, the equations for Ω_{ij} are

$$\frac{d\Omega_{ij}}{dt} = -\Omega_{ik}s_{kj} - s_{ik}\Omega_{kj} + \nu \Delta \Omega_{ij}. \tag{2.10}$$

A set of Eqs. (2.7) and (2.10) determine the configuration of the microscopic structure of turbulence.

The microscopic structure of turbulence can be investigated in terms of s_{ij} and Ω_{ij}. Which quantity is more convenient for such an analysis? The symmetric strain tensor can be represented by d eigenvalues, while the antisymmetric tensor has $d(d-1)/2$ components. Hence, s_{ij} is more convenient to use for the analysis of high-dimensional turbulence. In the following we analyze the simulated results for three to five dimensions with the aid of s_{ij}.

III. EIGEN VALUES OF THE STRAIN FIELD

We integrate numerically the Navier-Stokes Eq. (2.1) in decaying turbulence in spatial dimension 3, 4, and 5 by using the spectral method and investigate the distributions of eigenvalues of the strain tensor from a point of view of comparing those among different dimensions. The initial velocity field is Gaussian random with zero mean and has the energy spectrum

$$E_d(k) \propto (k/k_0)^{d+1} \exp\left[-\tfrac{1}{2}(k/k_0)^2\right],$$

where

$$E(t) = \frac{1}{2}\langle \mathbf{u}^2(t) \rangle = \frac{d}{2}u_{\rm rms}^2 = \int_0^\infty E(k,t)\, dk$$

and k_0 is the wavenumber of the energy spectrum peak. The details of the numerical integration are the same as in Refs. [9,10,13].

In order to have a meaningful comparison among different dimensions we simulated Eq. (2.1) on the grid points 64^d, and the data are sampled at the time slightly after the energy dissipation rate becomes maximum, R_λ being 16.2 then for all the runs. In order to obtain better statistical convergence in 3 dimensions, we took an average over ten runs with different random initial conditions.

The eigenvalues $\tilde{\lambda}_i$ of s_{ij} are computed on each mesh point. For convenience we normalize $\tilde{\lambda}_i$ in such a way,

$$\lambda_i = \frac{\tilde{\lambda}_i}{\sqrt{\sum_i \tilde{\lambda}_i^2}} = \frac{\tilde{\lambda}_i}{\sqrt{\bar{\epsilon}/2\nu}},$$

where $\bar{\epsilon}$ is the average rate of the energy dissipation.

The normalized eigenvalues are ordered in such a way that $\lambda_1 > \lambda_2 > \cdots > \lambda_d$. The incompressibility condition demands that $\sum_i \lambda_i = 0$, so that $\lambda_1 > 0$ and $\lambda_d < 0$ always. The intermediate eigenvalues can take any sign.

A. Probability distribution of the eigenvalues

In Fig. 1 we depict the PDF's of eigenvalues for $d = 3$, 4, and 5. Looking at those three figures we notice that the PDF's

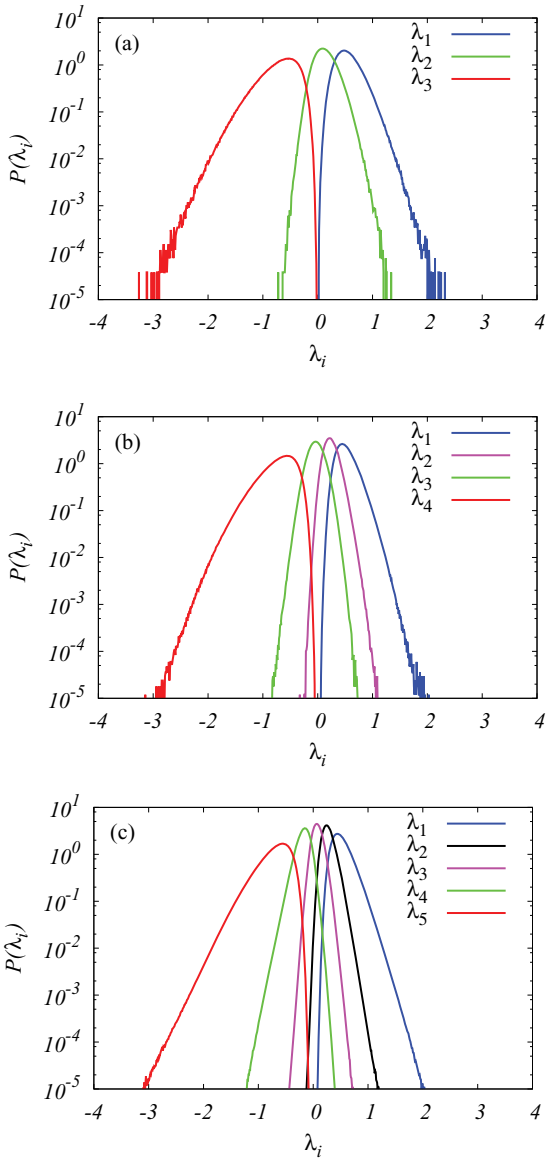

FIG. 1. (Color online) Normalized PDF of λ_i at $R_\lambda = 16.2$. Peaks of the curves are for $\lambda_1, \ldots, \lambda_d$ from the rightmost. (a) 3D, (b) 4D, (c) 5D.

of the lowest eigenvalue λ_d and the highest one λ_1 look like the same for all dimensions. To confirm it, the PDF's of λ_d and λ_1 of different dimensions are compared in Fig. 2. The findings are as follows. (1) PDF's of λ_d and λ_1 are asymmetric about their peaks, (2) PDF of λ_d is wider than that of λ_1, (3) PDF's of the intermediate eigenvalues tend to become approximately symmetric and narrower and tend to evenly distribute between the PDF's of λ_d and λ_1 when the spatial dimension increases, (4) PDF's tend to decrease exponentially at far tail with increase of the spatial dimension, (5) the PDF shape of λ_d is insensitive to the variation of the spatial dimension, suggesting that the compression mechanism is universal irrespective of the dimension, (6) the PDF shape of λ_1, on the other hand, depends slightly on the spatial dimension. In particular, the distribution in 5D is narrower than that in 3D, and the PDF in 4D is narrower than those for odd dimensions. It is not clear at present whether the additional invariants depending on the

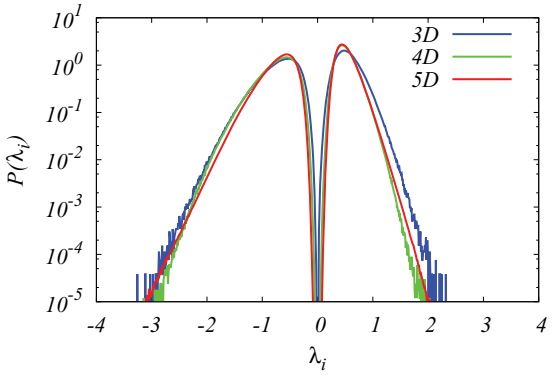

FIG. 2. (Color online) Normalized PDF's of the lowest and the highest eigenvalues for various dimensions at the same Reynolds number $R_\lambda = 16.2$. Curves of $\lambda_1 > 0$ are for 3D, 5D, and 4D from the uppermost at $\lambda_1 = 1.5$, respectively. Curves of λ_d are for 3D, 4D, and 5D from the uppermost at $\lambda_d = -2$, respectively.

parity of the dimension affect the result [8]. In this context, 6D turbulence may answer this issue. Observation (2) is consistent with the negative skewness $\langle(\partial_1 u_1)^3\rangle/\langle(\partial_1 u_1)^2\rangle^{3/2}$, which is a measure of the energy transfer to small scales of motion. The above observations suggest that λ_d, the most negative eigenvalue, plays an important key role, which will be seen in the following.

B. Conditional average

The PDF's in Fig. 1 cannot give any account of how the eigenvalues of different sign distribute on grid points. Consider a case of three dimensions, for instance, where the types of eigenvalues $(+,-,-,)$ and $(+,+,-,)$ are possible. It is not meaningful to count the number of two types without restrictive condition. We would like to find a degree of correlation between the appearing rate of those types and the level of activeness in turbulence. Since $\langle\sum_i \tilde{\lambda}_i^2\rangle = \bar{\epsilon}/2\nu$, the local level of turbulent activeness is high where the magnitude of λ_d and λ_1 are large. Here we choose the smallest eigenvalue λ_d as the representative of the level of turbulence.

1. 3D

In 3D, another simulation was made on 512^3 grid points, the data being sampled at $R_\lambda = 53.7$. In Fig. 3(a) the appearing rate of two types of pattern $(+,+,-)$ and $(+,-,-)$ for $\lambda_3 < x$ is given as a function of x. We notice that the pattern $(+,+,-)$ is dominant any time. The above result indicates that the sign of λ_2 is strongly governed by the magnitude of λ_3. In order to know the correlation between λ_2 and λ_3, we plotted a set of (λ_2,λ_3) observed on all grid points in Fig. 4, where every 40 points are plotted to reduce the figure size. Notice that there is a distinct anticorrelation between both eigenvalues; λ_2 increases statistically as λ_3 decreases. From the distributions of (λ_1,λ_3) and (λ_2,λ_3) we compute the conditional averages of λ_1 and λ_2 for a given value of λ_3 as

$$\begin{aligned}\langle\lambda_1|\lambda_3\rangle &= -0.67\lambda_3 + 0.094,\\ \langle\lambda_2|\lambda_3\rangle &= -0.33\lambda_3 - 0.094,\end{aligned} \tag{3.1}$$

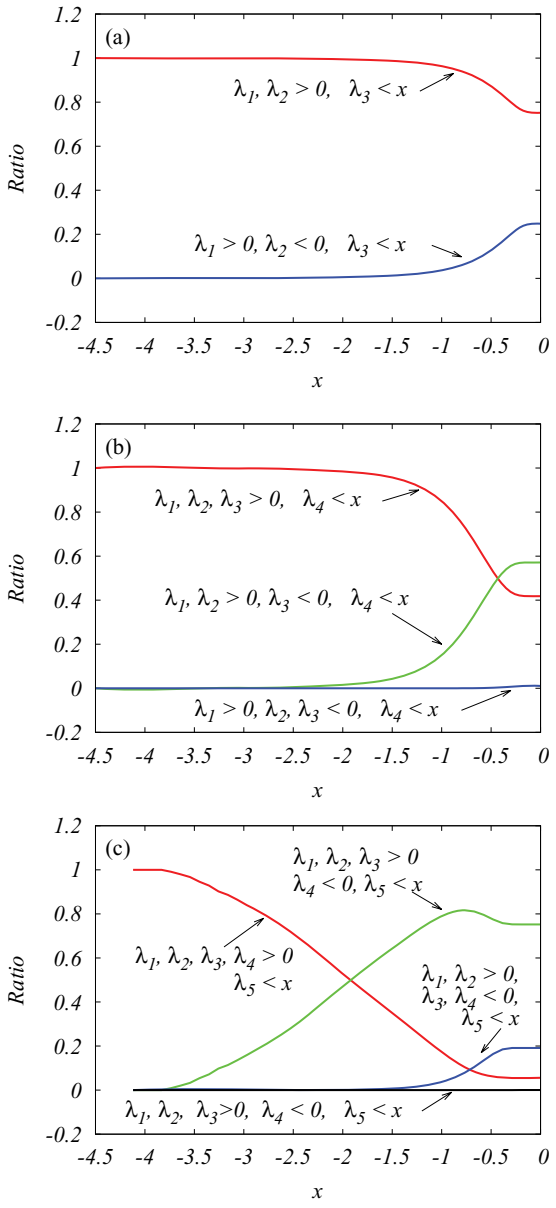

FIG. 3. (Color online) Appearing rate of two, three, and four types for λ_d in $d = 3$, 4, and 5, respectively. (a) 3D at $R_\lambda = 53.7$, (b) 4D at $R_\lambda = 21.1$, (c) 5D at $R_\lambda = 16.2$.

where the constants were determined by the least square fitting over the range $-3 < \lambda_3 < -0.5$. When the fitting range was changed to $-3.5 < \lambda_3 < -1.0$, it was found that the slopes varied about 10% and the constants about 20% reflecting the small Reynolds number and the finiteness of sample points, especially for large $|\lambda_3|$. This trend is also applied to higher dimensions. However, the variation of the constants does not affect the arguments in what follows.

The incompressible condition $\langle\lambda_1|\lambda_3\rangle + \langle\lambda_2|\lambda_3\rangle + \lambda_3 = 0$ is satisfied even statistically. The first member shows $\langle\lambda_1|\lambda_3\rangle > 0$ as it should be. The second member of Eq. (3.1) means that a region with a large value of $|\lambda_3|$ tends to have positive value of λ_2, statistically speaking, which is in accordance with the result derived from Fig. 3(a). We call such a set of points

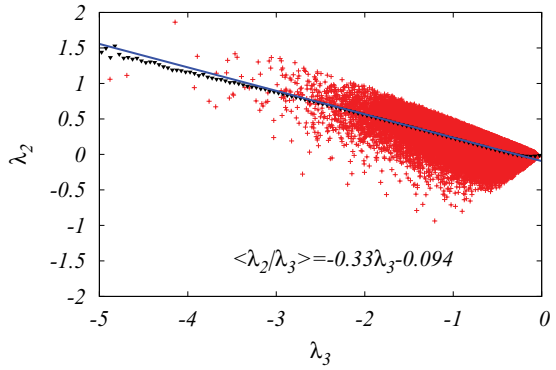

FIG. 4. (Color online) Scatter plot (plus) of λ_2 against λ_3 in 3D at $R_\lambda = 53.7$. Triangles are the average value of λ_2 for given λ_3, and the straight line is the linear regression curve fitted over the range $[-3, -0.5]$.

as the active region where there exists a single direction of compression and the type $(+, +, -)$ prevails. As is clearly seen in Fig. 4 the distribution of points is bounded by two straight lines; $\lambda_2 = \lambda_3$ for the lower boundary and $\lambda_2 = -\lambda_3/2 (\lambda_1 = \lambda_2)$ for the upper one, which are easily obtained by noting that $\lambda_1 > \lambda_2 > \lambda_3$ and $\lambda_1 + \lambda_2 + \lambda_3 = 0$. It is also possible to choose λ_1 instead of λ_3 as the representative. However, since the action to squeeze a fluid blob is closely related to the energy transfer to smaller scales, we employ the lowest eigenvalue λ_d as the reference parameter in treating four and five dimensions afterward.

2. 4D

In 4D, an additional simulation was done on the grid points 128^4 and the data were sampled at $R_\lambda = 21.1$, which is about 40% of that in 3D. Three types $(+, -, -, -)$, $(+, +, -, -)$, and $(+, +, +, -)$ are possible in principle. We plot the appearing rate of those types for $\lambda_4 < x$ against x in Fig. 3(b). For $\lambda_4 < -1$, the type $(+, +, +, -)$ becomes predominant. From the plots of $\lambda_1, \lambda_2, \lambda_3$ against λ_4 as in Fig. 4, we obtain the following relationships:

$$\begin{aligned} \langle\lambda_1|\lambda_4\rangle &= -0.51\lambda_4 + 0.12, \\ \langle\lambda_2|\lambda_4\rangle &= -0.28\lambda_4 - 0.03, \\ \langle\lambda_3|\lambda_4\rangle &= -0.21\lambda_4 - 0.15, \end{aligned} \tag{3.2}$$

over the range $-3.0 < \lambda_4 < -0.5$. The first two conditional averages $\langle\lambda_1|\lambda_4\rangle$ and $\langle\lambda_2|\lambda_4\rangle$ are positive except for a small value of $|\lambda_4|$, while $\langle\lambda_3|\lambda_4\rangle$ is positive for $\lambda_4 < -0.71$. Hence, the active region is characterized by a type $(+, +, +, -)$, suggesting a single direction of compression there.

3. 5D

In 5D, the simulation was done on the grid points 64^5 and the data sampling at $R_\lambda = 16.2$. Four types $(+, -, -, -, -)$, $(+, +, -, -, -)$, $(+, +, +, -, -)$, and $(+, +, +, +, -)$ are possible. The appearing rates of those types are given against λ_5 in Fig. 3(c). For $\lambda_5 < -2$, the type $(+, +, +, +, -)$ becomes dominant. Again, we plot the distribution of $\lambda_1, \lambda_2, \lambda_3$, and λ_4 against λ_5, as in Fig. 4, and obtain the

conditional averages as

$$\begin{aligned}\langle\lambda_1|\lambda_5\rangle &= -0.47\lambda_5 + 0.16,\\ \langle\lambda_2|\lambda_5\rangle &= -0.23\lambda_5 + 0.12,\\ \langle\lambda_3|\lambda_5\rangle &= -0.16\lambda_5 + 0.03,\\ \langle\lambda_4|\lambda_5\rangle &= -0.13\lambda_5 - 0.29,\end{aligned} \tag{3.3}$$

over the range $-3.0 < \lambda_5 < -0.5$. It should be noted that when i increases, the proportional constant a_i decreases initially but the decay rate becomes smaller. Consequently, λ_1,λ_2, and λ_3 are statistically positive. The sign of λ_4 depends on the magnitude of λ_5; it is positive in the region where $\lambda_5 < -2.2$. Hence, in the strongly active region, only the type $(+,+,+,+,-)$ is possible.

IV. STRUCTURE OF VELOCITY 2-FORM FIELD

Now let us turn to the velocity 2-form Ω_{ij}, the antisymmetric tensor of the velocity gradient. It is known that in three dimensions Ω_{ij} is related to the vorticity by Eq. (2.6) and ω tends to align the direction parallel to the eigenvector belonging to λ_2. In d dimensions, however, it is difficult and may not be effective to examine which eigenvector is correlated to Ω_{ij}, especially for large d. Instead we examine the statistical dependence between the local strain field and the enstrophy in d-dimensional turbulence, which is defined as

$$Q_1 = \tfrac{1}{4}\Omega_{ij}^2. \tag{4.1}$$

Correspondingly, we consider also the total squared strain

$$Q_2 = s_{ij}^2, \tag{4.2}$$

which is equal to $\epsilon/2\nu$. In the instantaneous diagonal framework, the above two quantities are

$$Q_1 = \tfrac{1}{4}\Omega_{ij}^2, \quad Q_2 = \lambda_j^2, \tag{4.3}$$

where Ω_{ij} is understood as the one transformed in terms of the orthogonal matrix. The Q_1 and Q_2 are related to the pressure by Eq. (2.8), which now becomes

$$\Delta p = Q_1 - Q_2 \equiv Q. \tag{4.4}$$

As in the previous section, we consider the conditional averages $\langle Q_1|\lambda_d\rangle$ and $\langle Q_2|\lambda_d\rangle$ for a given value of the most compressible eigenvalue λ_d of the strain tensor. By projecting Q_1 and Q_2 on the most negative eigenvalue λ_d, we can infer to what extent the locally compressed action of the strain field is responsible for the pressure, enstrophy, and so on.

We have computed the conditional averages Q_1 and Q_2 as functions of λ_3 by the three-dimensional simulation with 512^3 grid points at $R_\lambda = 68.6$. Figure 5 depicts the scatter plots (dots) and the conditional averages (symbols) and the fitted lines of (a) $\langle Q_1|\lambda_3\rangle$, (b) $\langle Q_2|\lambda_3\rangle$, (c) $\langle Q|\lambda_3\rangle$, and (d) close up view near the origin as functions of λ_3, where λ_3 is normalized by $\sqrt{\sum_i \lambda_i^2} = \sqrt{\overline{\epsilon}/(2\nu)}$, and Q_1, Q_2, Q by $\overline{\epsilon}/(2\nu)$. Because the number of data is enormous, every 2×10^4 points was plotted to save the data size in the scatter plots. A large number of points are located in the region $|\lambda_3| < 3$, but still many points are outside the region, although they are not clearly seen in the figures because of the substantial reduction of points.

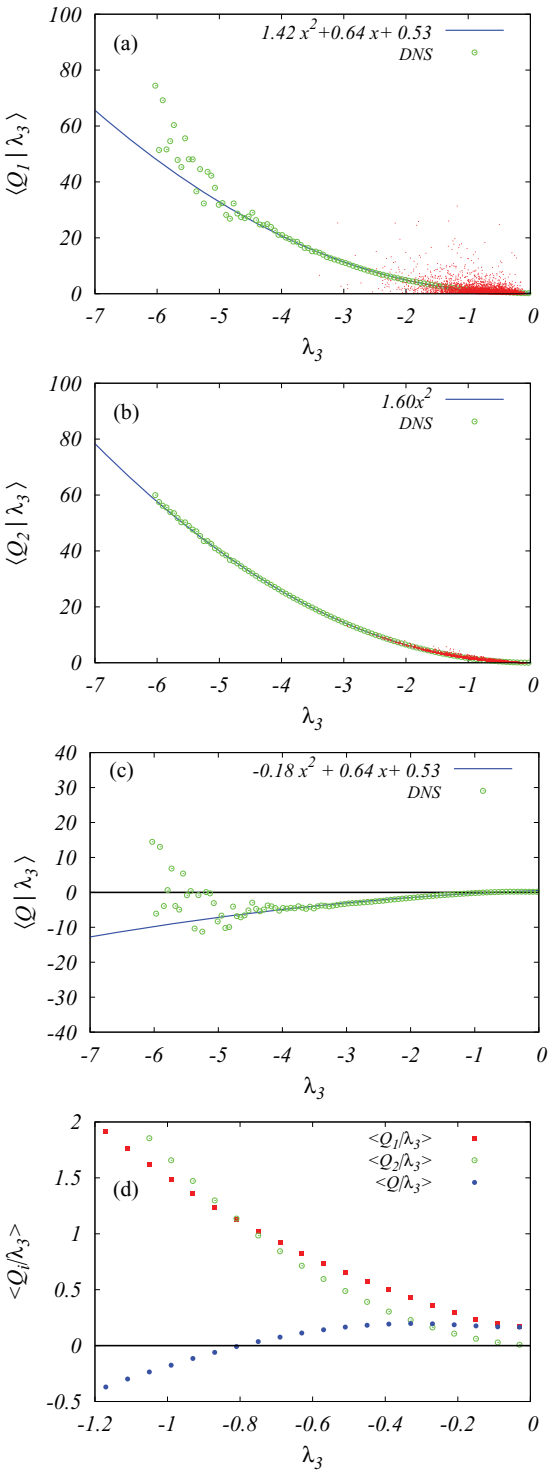

FIG. 5. (Color online) Scatter plots and conditional averages of (a) $\langle Q_1|\lambda_3\rangle$, (b) $\langle Q_2|\lambda_3\rangle$, and (c) $\langle Q|\lambda_3\rangle$ as function of λ_3 in 3D. (d) Close up of the conditional averages near the origin obtained by DNS. Dots, each point; symbols, the conditional average of DNS; lines, the best fitting curve. In (d): square, $\langle Q_1|\lambda_3\rangle$; open circle, $\langle Q_2|\lambda_3\rangle$; filled circle, $\langle Q|\lambda_3\rangle$. λ_3 is normalized by $\sqrt{\sum_i \lambda_i^2} = \sqrt{\overline{\epsilon}/(2\nu)}$, and Q_1, Q_2, and Q by $\overline{\epsilon}/(2\nu)$.

In Fig. 5(a), the scatter of the data points is large, which indicates that the enstrophy Q_1 is not governed restrictively by λ_3. The vorticity is significantly large even where $|\lambda_3|$ is not

large. It is very probable that the vorticity diffuses from the region where it is amplified by the strong strain field into the region where the strain field is very weak. From the close-up view of Fig. 5(d) it follows that $\langle Q_1|\lambda_3\rangle$ is finite and positive at $|\lambda_3| \ll 1$. The curve is fitted as

$$\langle Q_1|\lambda_3\rangle = 1.42\lambda_3^2 + 0.64\lambda_3 + 0.53 \tag{4.5}$$

over the range $-5 < \lambda_3 < 0$. When the fitting range was changed to $-4 < \lambda_3 < 0$, three constants vary within 15%.

Figure 5(b) shows the scatter plot and the conditional average $\langle Q_2|\lambda_3\rangle$ (symbols). The scatter of the data points from the conditional average is very small when compared to $\langle Q_1|\lambda_3\rangle$ as expected from the definition of Q_2 (4.3). It should be noted that (1) $\langle Q_1|\lambda_3\rangle$ grows faster than $\langle Q_2|\lambda_3\rangle$ with increase of $|\lambda_3|$, on the other hand, (2) $\langle Q_2|\lambda_3\rangle$ vanishes and has zero slope at the origin but is larger than $\langle Q_1|\lambda_3\rangle$ for the moderate value of $|\lambda_3|$ as seen from Fig. 5(d). The conditional average is beautifully fitted in the range $-5 < \lambda_3 < 0$ by the curve

$$\langle Q_2|\lambda_3\rangle = 1.60\lambda_3^2, \tag{4.6}$$

which is consistent with the value evaluated from the result Eq. (3.1) with the small constant terms being ignored. When the fitting range is changed to $-4 < \lambda_3 < 0$, the constant varies about 0.1%.

The sum Q is depicted in Fig. 5(c). The fitting curve is computed as

$$\langle Q|\lambda_3\rangle = -0.18\lambda_3^2 + 0.64\lambda_3 + 0.53 \tag{4.7}$$

by subtracting Eq. (4.6) from Eq. (4.5). The fitted curve follows well the numerically obtained $\langle Q|\lambda_3\rangle$. In Fig. 5(d), $\langle Q|\lambda_3\rangle$ by DNS for $-0.5 < \lambda_3 < 0$ is approximately constant at about 0.17, while the constant 0.53 of Eq. (4.7) is larger by about three times. This difference implies that Q_1 is independent of small $|\lambda_3|$.

It follows that the magnitude of $\langle Q|\lambda_3\rangle$ is much smaller than $\langle Q_1|\lambda_3\rangle$ and $\langle Q_2|\lambda_3\rangle$ up to $\lambda_3 = -7$ due to the cancellation. It should be stressed that this does not necessarily mean that at each grid point the cancellation occurs. Although $\langle Q_1|\lambda_3\rangle$ grows in proportion to $-0.18\lambda_3^2$, the PDF of λ_3 decays rapidly for large negative λ_3 as seen in Fig. 1(a) so that the average vanishes:

$$\langle Q\rangle = \int_{-\infty}^{0} \langle Q|\lambda_3\rangle P(\lambda_3) d\lambda_3 = 0. \tag{4.8}$$

Indeed, we confirmed that $\langle Q\rangle = 3.5 \times 10^{-16}$ in the simulation.

Unfortunately, the above analysis has not been made for the dimensions 4 and 5. However, effects of the spatial dimension on Q_1, Q_2, and Q may be inferred from the PDFs $P(Q)$ of Q plotted in Fig. 6 for dimension $d = 3,4$, and 5, which are computed at the same Reynolds number $R_\lambda = 16.2$. In any dimension, the PDF tail on the positive side of Q is longer than that on the negative side. It means that the intense Ω_{ij} is more probable than the strain field, which is consistent with the observation of Fig. 5. When the dimension increases, the right tail becomes shorter while the left tail becomes slightly longer, so that the asymmetry of the PDF becomes weaker. Since the pressure is determined by the Poisson equation [Eq. (4.4)], the shorter positive tail of $P(Q)$ means that the probability

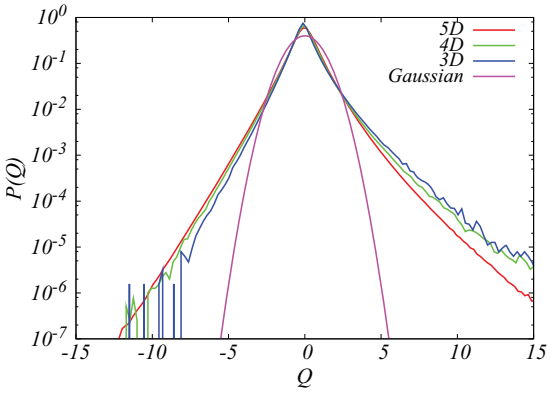

FIG. 6. (Color online) PDF of Q for dimensions from 3 to 5. The abscissa is normalized in terms of the standard deviation of Q. Curves on the positive side are for 3D, 4D, and 5D from the uppermost at $Q = 7$, respectively. Curves on the negative side are for 5D, 4D, and 3D from the uppermost at $Q = -7$, respectively. The parabola is the Gaussian PDF.

of finding the large negative pressure events becomes smaller, which in turn leads to less probability of the large enstrophy Q_1 (vorticity). On the other hand, the longer negative tail of $P(Q)$ means that the probability of the large positive pressure increases and so does for the probability of the large total squared strain Q_2 (dissipation). The effects of dimension appear stronger on the right tail than on the left. This can be understood as follows. In the local diagonal framework of the strain tensor, Q_1 is given by the sum of $d(d-1)/2$ terms, while Q_2 has d terms from Eq. (4.3). Therefore, when d becomes large, the central limit theorem applies stronger to Q_1 than Q_2, so that the right tail of $P(Q)$ becomes shorter and the left tail tends to be slightly longer, yielding a symmetric PDF of Q with the exponential tail, which would be the one resulting from the Gaussian random velocity field [10].

V. DISCUSSION AND CONCLUSION

The conditional average of the eigenvalue of the strain tensor in 3, 4, and 5 dimensions is well approximated as the linear function of λ_d: $\langle\lambda_i|\lambda_d\rangle = -a_i\lambda_d + b_i$, where a_i are positive definite while b_i change sign randomly. The incompressibility condition implies the constraints $a_1 + a_2 + \cdots + a_{d-1} = 1$, and $b_1 + b_2 + \cdots + b_{d-1} = 0$. The former condition is well satisfied for all dimensions $d = 3,4$, and 5, while the latter is satisfied only approximately. The Reynolds number dependence of a_i is not known. One interesting observation is the fact that the constant a_i decreases as i increases but tends to saturate for large i. There seem two possibilities that (A) the large compression is balanced by $d-1$ similar amplitudes stretching, or (B) the large compression with λ_d is countered mainly by a single large stretching motion with λ_1 accompanied by several small positive stretching $\lambda_i (i = 2, \ldots, d-1)$. Although our DNS data are not enough to definitely determine which case is more probable, it is interesting to examine how the energy is dissipated in both cases. First, we consider case (A). In this case, the simplest model for a_i is to put $a_i = 1/(d-1)$. In the active region where b_i term is small compared to

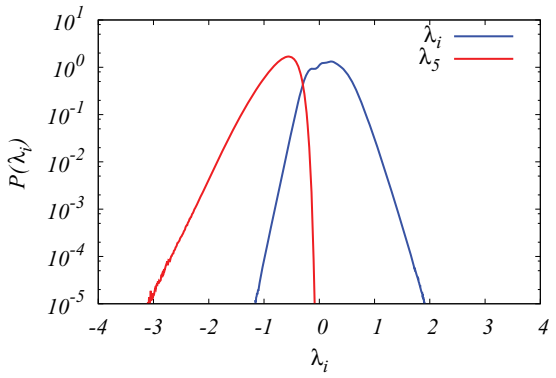

FIG. 7. (Color online) Normalized PDF's of λ_d (left curve) and the collection (right curve) of the remaining components in 5D.

the linear term $-a_i\lambda_d$, the local energy dissipation rate $\varepsilon(\mathbf{x})$ is expressed as $\varepsilon = 2\nu(\sum_i^{d-1} a_i^2 + 1)\lambda_d^2 = 2\nu c_d \lambda_d^2$, where $c_d = d/(d-1)$. If we substitute Eqs. (3.1) to (3.3) into this expression, we obtain $c_d^{\mathrm{DNS}} = 1.56, 1.38, 1.34$ for $d = 3,4,5$, respectively, while the theoretical values c_d are $1.5, 1.33, 1.22$ for $d = 3,4,5$, respectively, which are close to the DNS values. In the large limit of d, the energy dissipation occurs mostly in a small space perpendicular to the eigenvector corresponding to λ_d. Next, we consider case (B). The simplest model is to put $\lambda_i = 0, (i = 2, \ldots, d-1)$, so that $\lambda_d = -\lambda_1$, which is similar to the case in two dimensions, and the energy dissipation is $\varepsilon = 4\nu\lambda_d^2$. However, this is a rather extreme case.

The PDF of the collected eigenvalues $\{\lambda_i\}$ other than λ_d in 5D is plotted in Fig. 7. We see that the PDF of the remaining eigenvalues is similar to that of λ_d when the sign is inverted but with rather rounded peak, which implies that λ_d competes with the other components. From the previous consideration and the PDF's of eigenvalues in 5D in Figs. 1(c) and 7, we are lead to consider that case (A) is more plausible than case (B), and that the smallest eigenvalue λ_d overwhelms other components in any dimension and that the flow comes in along a direction of the smallest eigenvalue and comes out toward other directions, the Burgers dynamics in d dimensions. This picture is also consistent with the theoretical prediction by Refs. [1,9–11].

The conditional averages of the enstrophy and the total squared strain in three dimensions are found to be increasing functions of λ_3. It is found that $\langle Q_1|\lambda_3\rangle$ grows faster than $\langle Q_2|\lambda_3\rangle$ for large negative λ_3. The PDF of the source term of the Poisson equation of the pressure is found to be positively skewed and approaches a symmetric PDF as the dimension increases. This is due to the relatively faster increase of the number of terms involved in the enstrophy (right tail) than that of the total squared strain (left tail).

The above observations and theoretical considerations lead us to conclude that when the spatial dimension increases the enhanced compression in one direction and the weak expansion in other (many) directions tend to dominate the dynamics and the enhanced energy transfer, the Burgers dynamics in d dimensions. Therefore, the compression along the direction is a driving motor of turbulence.

ACKNOWLEDGMENTS

The authors express their thanks to the Theory and Computer Simulation Center of the National Institute for Fusion Science (Grant No. NIFS10KNSS008). T.G. was supported by Grants-in-Aid for Scientific Research No. 21360082 and No. 24360068 from the Ministry of Education, Culture, Sports, Science and Technology of Japan.

[1] M. Nelkin, Phys. Rev. A **11**, 1737 (1975).
[2] U. Frisch, M. Lesieur, and P. L. Sulem, Phys. Rev. Lett. **37**, 895 (1976).
[3] J. D. Fournier and U. Frisch, Phys. Rev. A **17**, 747 (1978).
[4] J. D. Fournier, U. Frisch, and H. A. Rose, J. Phys. A **11**, 187 (1978).
[5] V. Yakhot, Phys. Rev. E **63**, 026307 (2001).
[6] V. S. L'vov, A. Pomyalov, and I. Procaccia, Phys. Rev. Lett. **89**, 064501 (2002).
[7] U. Frisch, A. Pomyalov, I. Procaccia, and S. S. Ray, Phys. Rev. Lett. **108**, 074501 (2012).
[8] B. A. Khesin and Ya. V. Chekanov, Physica D **40**, 119 (1989).
[9] E. Suzuki, T. Nakano, N. Takahashi, and T. Gotoh, Phys. Fluids **17**, 081702 (2005).
[10] T. Gotoh, Y. Watanabe, Y. Shiga, T. Nakano, and E. Suzuki, Phys. Rev. E **75**, 016310 (2007).
[11] G. Falkovich, I. Fouxon, and Y. Oz, J. Fluid Mech. **644**, 465 (2010).
[12] P. G. Saffman, *Vortex Dynamics* (Cambridge University Press, Cambridge, 1992).
[13] T. Gotoh, D. Fukayama, and T. Nakano, Phys. Fluids **14**, 1065 (2002).